Ellipsometric studies of the dielectric function of $Cd_{1-x}Mn_xTe$ alloys

P. Lautenschlager, S. Logothetidis,* L. Viña,† and M. Cardona
Max-Planck-Institut für Festkörperforschung, Heisenbergstrasse 1, D-7000 Stuttgart 80, Federal Republic of Germany
(Received 10 May 1985)

We present ellipsometric measurements of the dielectric function of a series of $Cd_{1-x}Mn_xTe$ samples ($0<x<0.7$) in the (1.5—5.5)-eV photon-energy region at room temperature. The data display structures which can be attributed to the E_0, $E_0+\Delta_0$, E_1, $E_1+\Delta_1$, and E_2 critical points of zinc-blende-type semiconductors: A fit of these structures with standard analytic expressions yields the energies, widths, strengths, and excitonic phase angles of the critical points. While the energy of the E_0 critical points increases with x, those of E_1 and $E_1+\Delta_1$ *decrease* slightly. This fact is probably related to an increasing admixture of spin-up Mn $3d$ states into the initial valence states of these transitions.

I. INTRODUCTION

A number of $3d$ transition-metal atoms can be built substitutionally into cation sites of II-VI compound semiconductors with zinc-blende structure (ZnS, ZnSe, ZnTe, CdTe, HgSe, and HgTe). The corresponding electronic levels are expected to be strongly affected by intra-atomic exchange and correlation effects (configuration interaction) contrary to the situation for standard shallow donor and acceptor impurities.[1] Impurity levels located in the forbidden gap usually arise. The ordering of these levels is determined by the ligand field, exchange, and correlation effects, whereby remnants of the atomic Hund's rule often require the maximization of the total spin in the ground state.

Among the $3d$ transition metals Mn plays a special role. The free Mn atom has a $3d^5 4s^2$ configuration. Hence if one considers the $3d^5$ electrons as part of the core, Mn is chemically divalent and thus can be used to replace a cation in a II-VI compound. Moreover, according to Hund's rule the $3d^5$ electrons would all be expected to have their spins parallel (up). These levels should split under the ligand field into a triplet (t_2 or Γ_{15}) and a doublet (e or Γ_{12}). The ligand-field splitting (~ 1 eV) is usually smaller than the energy it takes to flip a spin against Hund's rule (~ 4 eV, spin splitting).

In ZnS and ZnSe, Mn ions substituting for Zn give levels in the forbidden gap: Relatively sharp optical transitions between occupied and empty levels (spin flip) are observed.[1,2] In the tellurides of Zn, Cd, and Hg, however, the occupied one-electron d levels seem to lie within the valence band,[3–5] their center being about 2.5 eV below the top of the valence bands.[4–5] Consequently the spin-up $3d^5$ levels of Mn must hybridize heavily with the $5p$ levels of Te. This hybridization probably contributes to the chemical bonding and thus to the wide solubility range of Mn in $Cd_{1-x}Mn_xTe$,[6] $Hg_{1-x}Mn_xTe$,[7] and $Zn_{1-x}Mn_xTe$.[8] The situation is somewhat similar to that which arises in the cuprous halides, except that in the latter the $3d$ shell of copper is completely filled as opposed to the Mn-compounds where the $3d$ shell is only half filled.[9]

The empty $3d$ levels of the Mn—group-II tellurides correspond to flipping one spin in the Hund ground state of the Mn. The spin-flip energy, about 5 eV,[3,4] is responsible for the insulating character of these materials: Within the framework of conventional one-electron band theory they would be metallic. It is, however, possible to treat the pure Mn compound (MnTe) within the framework of band theory by assuming that it is antiferromagnetic in the ground state, i.e., that the Mn atoms occupy two different sublattices, one with spin up and the other with spin down. The calculated band structure of this material in the hypothetical antiferromagnetic zinc-blende structure has been given in Ref. 4 (hypothetical in as far as pure MnTe is found only in the NiAs structure). $Cd_{1-x}Mn_xTe$ is found in the zinc-blende structure for $x \lesssim 0.8$. The band structure of MnTe in the naturally occurring antiferromagnetic NiAs structure has been presented in Ref. 10. This band structure is qualitatively similar to that of the hypothetical zinc-blende modification: it yields a spin-flip energy of about 5 eV and a ligand-field splitting of the $3d$ levels of 1—2 eV.

Information about the electronic excitation spectrum is most conveniently obtained by optical techniques. One must distinguish between the absorption edge, giving the threshold for excitations and corresponding to relatively weak absorption coefficients, and transitions above this edge which give the photon energies at which the strongest absorption processes occur (one or more orders of magnitude stronger than the absorption edge). The absorption edge of CdTe takes place between the top of the valence band (mainly Te $5p$ states) and the bottom of the conduction band (mainly Cd $5s$ states), both at the Γ point ($\mathbf{k}=\mathbf{0}$) of the Brillouin zone (BZ).[11] Upon substitution for Cd by Mn (i.e., increasing x in $Cd_{1-x}Mn_xTe$) this edge shifts linearly with x to higher energies.[12–15] Of particular interest is the fact that the absorption edge changes shape with increasing x.[12,14] In the high-absorption region ($\alpha > 10^4$ cm^{-1}) the edge shifts linearly up to the Mn solubility limit ($x \simeq 0.7$).[12,14] However, in the low-absorption region ($\alpha < 10^3$ cm^{-1}), the edge stops shifting and becomes independent of x for $x \gtrsim 0.5$.[12–15]

It is easy to interpret this fact as due to the existence of two sets of transitions in the neighborhood of the edge, one being the conventional transitions of CdTe and the other involving the empty, spin-flipped Mn $3d$ states as final states. The latter have been calculated to lie ~ 1 eV above the top of the valence band for $x=1$ using a local density functional,[4] a calculation which underestimates gaps by about 1 eV.[16] Hence we expect the excitation energy from the top of the valence band to the empty $3d$ states of Mn to be ~ 2 eV. The low-absorption part of the gap saturates at ~ 2.1 eV.[12,15] This interpretation of the gap of $Cd_{1-x}Mn_xTe$ is corroborated by measurements of the pressure dependence of the gap. The gaps for small x and their high-absorption coefficient for large x *increase* with pressure at a rate close to that for CdTe (7×10^{-2} eV/GPa) while the low-absorption component for $x>0.5$ *decreases* with increasing pressure at about half that rate.[17,18]

We note that in the $Zn_{1-x}Mn_xTe$ system the Te $5p\rightarrow$Zn $4s$ gap at Γ is higher than for $Cd_{1-x}Mn_xTe$ and thus the transitions to the spin-down Mn states can be seen at normal pressure for all values of x within the solubility range ($x\leqq 0.7$).[19]

Interband transitions in $Cd_{1-x}Mn_xTe$ above the absorption edge have been investigated by measuring the reflection spectra.[20–22] In these data, structure is identified which corresponds to the E_0, $E_0+\Delta_0$, E_1, $E_1+\Delta_1$, E_2, E_1', and $E_1'+\Delta_1'$ reflection peaks of CdTe.[23] The E_0 peak corresponds to the Te $5p\rightarrow$Cd $5s$ absorption edge at Γ, while $E_0+\Delta_0$ is its spin-orbit split component; E_1 and $E_1+\Delta_1$ represent transitions from the top, spin-orbit-split (Δ_1 denotes splitting) valence bands along $\langle 111\rangle$ (the Λ direction) of the BZ and the lowest conduction band along this direction; E_1' and $E_1'+\Delta_1'$ represent transitions between the same valence bands and the second-lowest conduction bands; E_2, the strongest peak in the reflection spectrum, corresponds to a set of transitions poorly localized in $\mathbf{k}$ space, which contain or are close to the lowest gap at the X point. According to Ref. 20 the Δ_0 spin-orbit splitting decreases slightly with x, a fact which is easy to attribute to the replacement of the weak Cd $5p$ component of the valence functions by Mn $3p$ upon increasing x. The splitting Δ_1 also decreases slightly with increasing x. The E_1 and $E_1+\Delta_1$ energies increase very weakly with doping, much less than E_0 and $E_0+\Delta_0$.[20] This behavior is somewhat anomalous when compared with other alloy zinc-blende–type systems which do not contain transition metals (see p. 483 in Ref. 24) and has remained unexplained hitherto.

In this paper we present ellipsometric measurements of the dielectric function of $Cd_{1-x}Mn_xTe$ in the 1.5–5.5 eV range. The dependence on x of the E_0, E_1, $E_1+\Delta_1$, and E_2 gaps is discussed. The critical energies corresponding to these gaps are accurately determined by fitting the observed spectra to theoretical expressions for the shape of the critical points. The data found for E_0 agree with previous results. We find, however, that the energies of E_1 and $E_1+\Delta_1$ decrease with increasing x: the anomaly suggested above for the data of Ref. 20 becomes clearer. This anomaly is explained as due to a repulsion of the upper valence bands along Λ by the occupied spin-up Mn $3d$ states which seem to be centered ~ 2.5 eV below the top of the valence band.

II. EXPERIMENT

Ellipsometric measurements were performed at room temperature with an automatic ellipsometer with rotating analyzer, as developed by Aspnes[25] and described elsewhere.[26] The ellipsometric data were processed with the two-phase model of the interface so as to obtain the approximate real and imaginary parts of the dielectric function (sometimes called "pseudo-dielectric-function" to distinguish it from the exact bulk dielectric function). The samples were grown by a modified Bridgman method with manganese concentrations of $x=0$, $x=0.10$, $x=0.20$, $x=0.45$, $x=0.65$, and $x=0.70$ without doping. The compositions have been checked by measuring the lattice constant, which varies linearly with composition as $6.487-0.149x$ (Å),[6] using x-ray powder diffraction. The samples were mounted in a windowless cell in flowing dry N_2, with the possibility to perform *in situ* etching procedures in order to minimize residual overlayers.

As shown by Aspnes[27] ellipsometric measurements of the dielectric function of zinc-blende–type semiconductors at the energy of the E_2 peak in ε_2 provide a sensitive indication of the dielectric discontinuity between sample and ambient. The ellipsometric parameters versus photon energy obtained with the largest value of ε_2 at the energy of the E_2 transitions are treated with the two-phase model[28] in order to obtain $\varepsilon_1(\omega)$ and $\varepsilon_2(\omega)$ of the semiconductor under study. In this sense, the best spectra for the samples with $x=0$ and 0.10 were obtained by cleaning the cleaved surface of the samples with methanol. For the samples with higher Mn concentration ($x\geqq 0.2$), the best spectra (i.e., the largest values of ε_2 in the ultraviolet region) were obtained from cleaved surfaces.

III. RESULTS

In Figs. 1 and 2 we show the real (ε_1) and imaginary part (ε_2) of the pseudo-dielectric-function for CdTe and three compositions of $Cd_{1-x}Mn_xTe$ ($x=0.20$, 0.45, and 0.70). These spectra were obtained from the measured complex reflectance ratios by using the two-phase model[28] in which the surface is treated as a plane boundary between two homogeneous media. The most important facts of these figures are the following. The E_0 peak in ε_1, which is below our experimental energy region for CdTe, shifts to higher energies with increasing composition x. A small shoulder corresponding to the $E_0+\Delta_0$ critical point at ~ 2.5 eV can be recognized for CdTe. The structures due to the E_1 and $E_1+\Delta_1$ transitions do not shift noticeably with increasing x but become much broader and hard to distinguish to the naked eye. The E_2 feature, well pronounced in CdTe, decreases and shifts to higher energies with increasing x and finally moves out of our spectral range.

To perform a line-shape analysis of the structures in our spectra, and thus to obtain the parameters of the critical points (CP's), the strength of the CP (A), the energy threshold (E), the broadening (Γ), and the excitonic phase

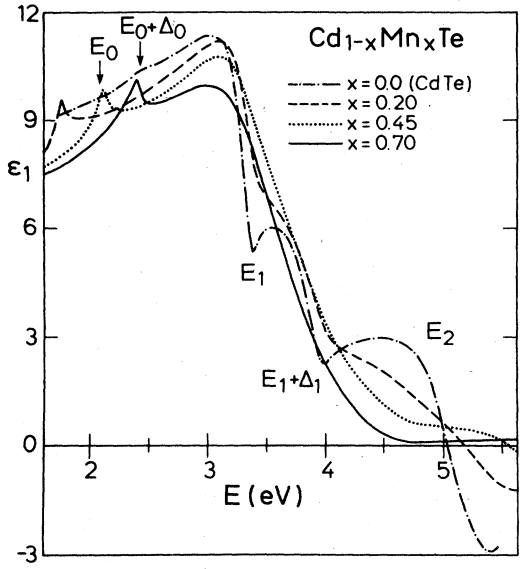

FIG. 1. Real part (ε_1) of the pseudo-dielectric-function of $Cd_{1-x}Mn_xTe$ with $x=0$, 0.20, 0.45, and 0.70 at room temperature.

angle (ϕ),[26] we calculate numerically[29] the second-derivative spectra of the dielectric function with respect to the photon energy, $d^2\varepsilon/d\omega^2$. The derivative spectra were fitted to one-electron CP line shapes.[26] A least-squares procedure was used for the fit, with both the real and the imaginary parts of $d^2\varepsilon/d\omega^2$ fitted simultaneously, except for the E_0 structure. Because of the poor accuracy of the values of ε_2 for small ε_2 in rotating analyzer ellipsometers without compensator,[30] we have analyzed the E_0 structure only in the derivative of the real part of the dielectric function. Excitonic effects can also be taken into account in a conventional manner by allowing a mixture of two

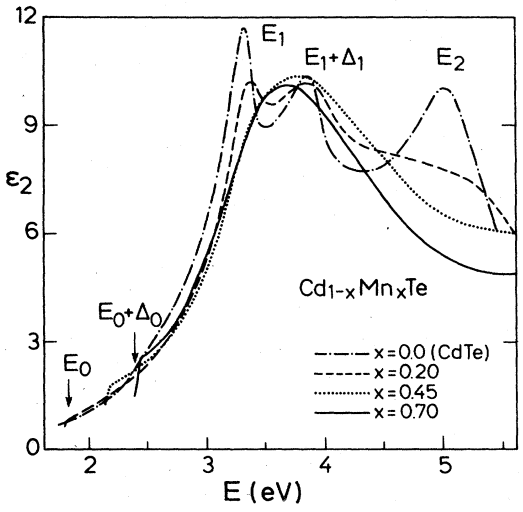

FIG. 2. Imaginary part (ε_2) of the pseudo-dielectric-function of $Cd_{1-x}Mn_xTe$ with $x=0$, 0.20, 0.45, and 0.70 at room temperature.

CP's.[31–33] The real part of the dielectric function in the E_0 region as well as the E_1, $E_1+\Delta_1$, and E_2 structures were best fitted with two-dimensional (2D) critical points, which can be represented by[31,33]

$$\varepsilon \sim C - \ln(E-\omega-i\Gamma)e^{i\phi}\,, \tag{1}$$

or for the second derivative

$$\frac{d^2\varepsilon}{d\omega^2} = -A(E-\omega-i\Gamma)^{-2}e^{i\phi}\,, \tag{2}$$

with the excitonic angle ϕ giving the amount of mixture of two critical points ($\phi=0$ for minimum, $\phi=\pi/2$ for saddle point, $\phi=\pi$ for maximum).

Figure 3 shows the fits of the second derivative of the real part of the dielectric function (open circles) to a two-dimensional minimum CP (solid line) and the resulting imaginary part for the E_0 transition. The E_1 and $E_1+\Delta_1$ features were fitted with a mixture of a 2D minimum or maximum and a saddle point. Typical results for $d^2\varepsilon_1/d\omega^2$ and $d^2\varepsilon_2/d\omega^2$ are shown in Fig. 4 with the experimental points given explicitly for $d^2\varepsilon_1/d\omega^2$. The arrows with question marks indicate weak structures in the

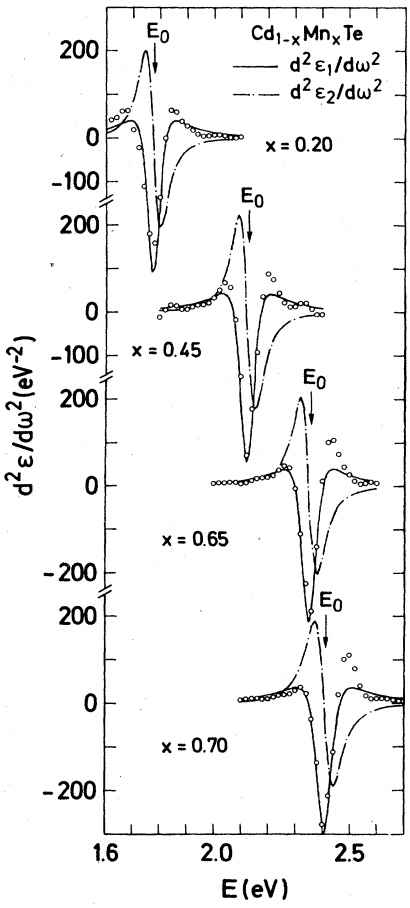

FIG. 3. Second derivative with respect to the photon energy of the real part of the pseudo-dielectric-function in the E_0 region. Points represent experimental data, the solid line the fit with a two-dimensional minimum CP, the dashed-dotted line the corresponding imaginary part.

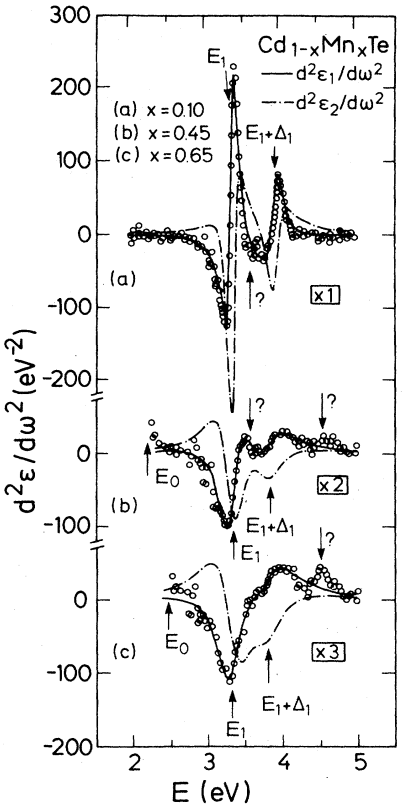

FIG. 4. Fits to the second derivatives of the real (solid line) and imaginary (dashed-dotted line) parts of the dielectric function of $Cd_{1-x}Mn_xTe$ as a function of photon energy. Dots represent data for $d^2\varepsilon_1/d\omega^2$. Vertical scale for $x=0.45$ has been expanded by a factor of 2, and that for $x=0.65$ by a factor of 3. Small structures with question marks have not been assigned to a CP.

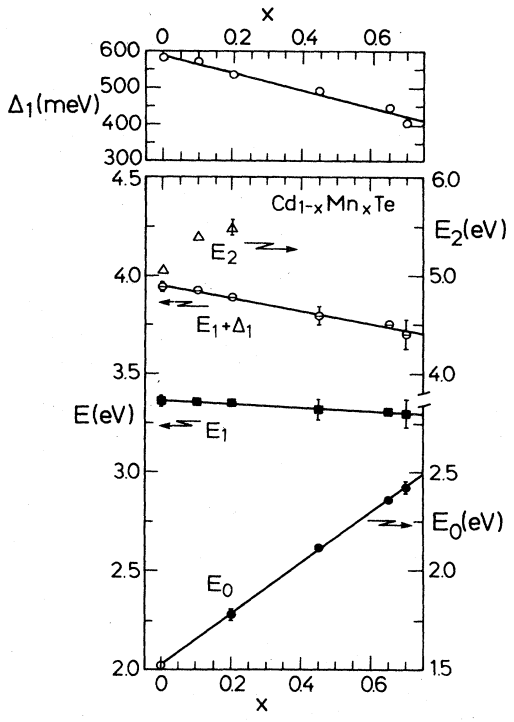

FIG. 5. Dependence of critical-point energies and spin-orbit splitting Δ_1 of $Cd_{1-x}Mn_xTe$ on composition x. Solid lines represent the best fits of our data to a linear function $[E(x)=a+bx]$.

experimental data, whose origin has not been identified.

The E_2 transitions fall within our spectral range only for three of our samples (up to $x \leqq 0.20$). In these cases they were fitted with a 2D maximum CP.

Figure 5 shows the energies of the E_0, E_1, $E_1+\Delta_1$, and E_2 CP's and Δ_1 (obtained by subtraction of the E_1 energy from that of $E_1+\Delta_1$) as a function of x. The results show in all cases a linear dependence of the gaps on concentration, the energy of E_0 increasing strongly with x, whereas the energies of E_1 and $E_1+\Delta_1$, as well as their spin-orbit splitting Δ_1, slightly decrease with x. The solid lines correspond to the best fit of our data to the expression

$$E(x)=a+bx \ . \tag{3}$$

The values of a and b for the E_0, E_1, and $E_1+\Delta_1$ structures, and for Δ_1 are listed in Table I.

The Lorentzian broadening parameters Γ for the E_0, E_1, and $E_1+\Delta_1$ CP's are displayed in Fig. 6. The broadening of the E_0 transition remains nearly constant, whereas those of E_1 and $E_1+\Delta_1$ increase strongly with increasing x. The solid lines are again the best fits to the linear equation $\Gamma(x)=a+bx$. The values of the coefficients can also be found in Table I.

In Fig. 7 we present the values of the excitonic phase angle ϕ versus composition obtained from our fits for E_1 (open circles) and the $E_1+\Delta_1$ (closed circles). For $180°>\phi>90°$ ($x<0.2$) the best fits correspond to a mixture of a 2D maximum and a saddle point. For $90°>\phi>0$ ($x>0.2$) the mixture is between a 2D minimum and a saddle point. The solid lines are the best

TABLE I. Values of the parameters a and b obtained by fitting the critical-point energy (E), the spin-orbit splitting Δ_1, and the Lorentzian broadening (Γ) vs composition (x) to the linear equations $E=a+bx$, $\Delta=a+bx$, and $\Gamma=a+bx$, respectively.

	a (eV)	b (eV)
E_0	1.53	1.26
E_1	3.36	−0.088
$E_1+\Delta_1$	3.95	−0.33
Δ_1	0.59	−0.24
Γ_{E_0}	0.054	−0.002
Γ_{E_1}	0.056	0.36
$\Gamma_{E_1+\Delta_1}$	0.115	0.42

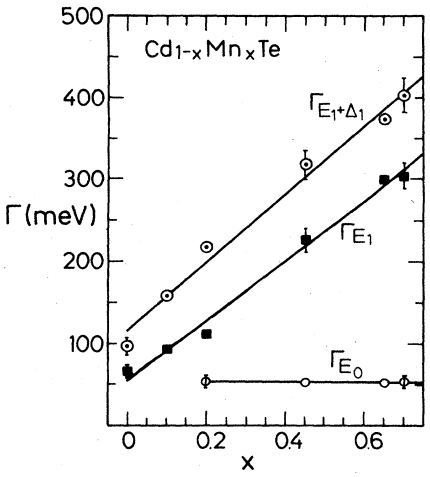

FIG. 6. Dependence of critical-point broadening parameters on composition. Solid lines are best fits to a linear function $[\Gamma(x)=a+bx]$.

fits to a quadratic equation

$$\phi(x)=\alpha+\beta x+\gamma x^2 ,$$

the corresponding coefficients being listed in Table II.

IV. DISCUSSION

Our critical-point energies agree generally with those of Ref. 20 except for the dependence of E_1 and $E_1+\Delta_1$ on x. In Ref. 20 an increase of these energies with x was reported while in Fig. 5 our results show a decrease of both energies with x. Also, in Ref. 20 Δ_1 decreases only very slightly with x, being nearly constant within the experimental scatter while our Fig. 5 shows a clear decrease of Δ_1 (from 600 to 400 meV in our range of x). We believe that these differences are due to the fact that in Ref. 20 the critical-point energies were taken to be those of the reflectivity maxima (which became shoulders for large x) while we have defined them through careful critical-point analysis of the second-derivative spectra. In order to check this hypothesis we have calculated the normal-incidence reflectivity spectra of our samples from the dielectric functions of Figs. 1 and 2 using Fresnel's relation: The results are displayed in Fig. 8. The position of the reflectivity maxima agree with the direct reflectivity measurements of Refs. 20 and 22 as indicated in Fig. 9.

We should point out that the increase in E_0 with x shown in Fig. 9 is in line with that expected from the systematics of other zinc-blende–type semiconductor al-

TABLE II. Values of parameters α, β, and γ obtained by fitting the excitonic phase angle (ϕ) to the quadratic expression $\phi=\alpha+\beta x+\gamma x^2$.

	α	β	γ
ϕ_{E_1}	152	−340	245
$\phi_{E_1+\Delta_1}$	158	−360	360

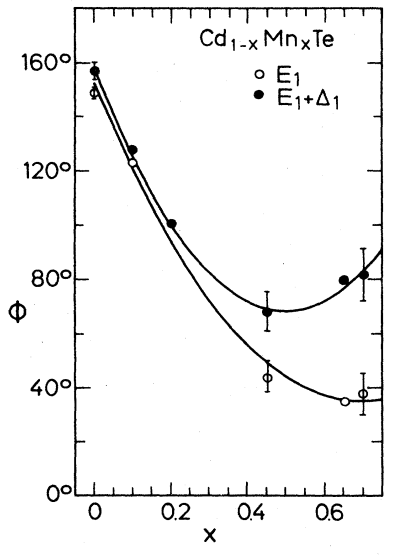

FIG. 7. Dependence on composition x of the excitonic parameter ϕ, defined in Eq. (1) for the E_1 (open circles) and the $E_1+\Delta_1$ (closed circles) critical points. Solid lines are fits to a quadratic function $[\phi(x)=\alpha+\beta x+\gamma x^2]$.

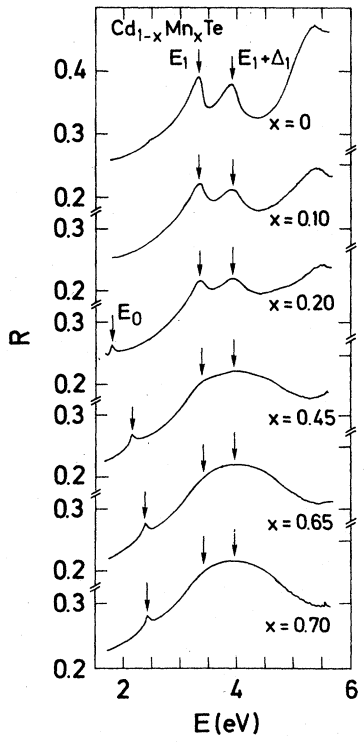

FIG. 8. Normal-incidence reflectivity spectra calculated from our measured dielectric function. Arrows indicate the peak position for the E_0, E_1, and $E_1+\Delta_1$ CP's.

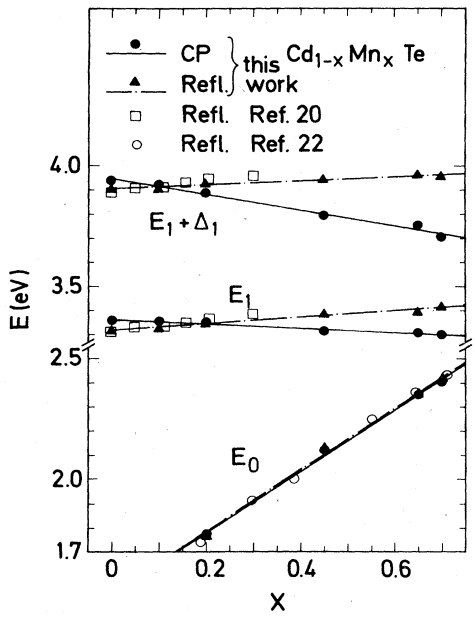

FIG. 9. Comparison between the CP energies obtained by line-shape analysis of the derivative spectra of ε (closed circles, with solid line as best linear fit) and by peak position of the reflectivity spectra (solid triangles, with dashed-dotted line as best linear fit). Open squares are reflectivity data for E_1 and $E_1+\Delta_1$ CP's from Ref. 20, the open circles those for the E_0 CP from Ref. 22.

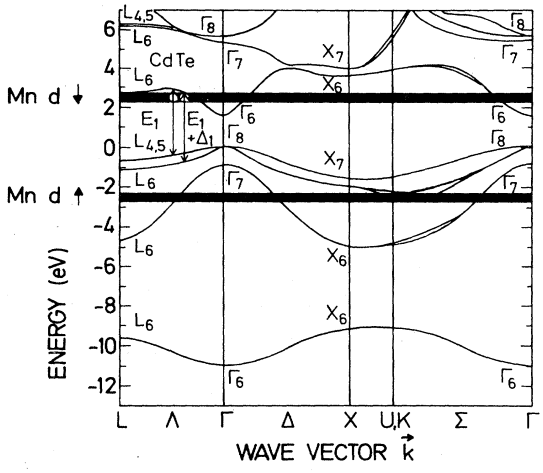

FIG. 10. Band structure for CdTe from Ref. 37. The additional $3d$ electron states of Mn are represented by the horizontal lines. Their position was taken from Ref. 4. For discussion, see text.

loys.[24,34] For instance, in $Cd_{1-x}Zn_xTe$, the nonmagnetic system which is closest to the one discussed here, the E_0 gap increases from 1.5 to 2.2 eV when x goes from 0 to 1.[24,35] Likewise, the E_1 gap increases from 3.3 to 3.6 eV. Hence the anomalous behavior of the $Cd_{1-x}Mn_xTe$ system becomes evident. For the sharper E_0 structure this problem does not arise (Fig. 9).

It is reasonable to seek a qualitative explanation of this behavior in the presence of the Mn $3d$ electrons. A schematic diagram of the position of these d electrons, prior to hybridization with the electronic states of Cd and Te, with respect to the energy bands of CdTe[36] is shown in Fig. 10. This position is derived from the calculations of Ref. 4 and the recent photoemission work of Ref. 37. We notice in Fig. 10 that the $d\uparrow$ and $d\downarrow$ states are *symmetrically* split with respect to the Γ_8 top of the valence bands of CdTe (mostly Te $4p$-like), hence the admixture of Mn $3d$ to the Γ_8 states should not appreciably shift the Γ_8 energy. Also, the mainly s-like wave functions of the lowest conduction-band minimum (Γ_6) should not mix with the Mn $3d$ states. Hence the admixture of Mn $3d$ states should not affect strongly the E_0 gap. The gap should thus increase with increasing x, as a result, at least in part, of the decrease in lattice constant. The situation is different for the E_1 and $E_1+\Delta_1$ gaps. The corresponding interband critical points, indicated by arrows in Fig. 10, take place along the ⟨111⟩ directions of **k** space. The $3d\uparrow$ levels are now below and rather close to the corresponding valence bands. Hence it is expected that the valence bands which participate in the E_1 and $E_1+\Delta_1$ transitions will be repelled to higher energies by the interaction with the Mn $3d$ levels as x is increased. This should lead to a decrease of these gaps, larger for $E_1+\Delta_1$ than for E_1, with increasing x provided the final conduction states (mainly cation s-like) do not mix much with the $3d$ states. This reasoning qualitatively explains the findings of Figs. 5 and 9. This mechanism will thus account, at least in part, for the decrease of the spin-orbit splitting Λ_1 with increasing x (Fig. 10). The decrease of Δ_0 (Ref. 20) can also be partly accounted for by a similar mechanism since the Γ_7 valence-band maximum should be repelled to higher energies while the Γ_8 maximum should remain nearly stationary. Another possible contribution to the decrease in Δ_0 and Δ_1 is the negative contribution of the spin-orbit splittings of the Mn $3d$ states to Δ_0 and Δ_1, a fact which has found clear confirmation in the cuprous halides.[38]

The Lorentzian broadenings found with the two-dimensional critical-point fit to the spectra of Fig. 4 are plotted versus x in Fig. 6. It is somewhat surprising that these broadenings vary linearly with x. In principle, if one attributes the increase in Γ to the disorder, one would expect it to have a maximum for $x\simeq 0.5$, the concentration at which the disorder should be a maximum. Nevertheless, the variation of the Γ at the E_1 and $E_1+\Delta_1$ critical points measured for $Cd_{1-x}Mn_xTe$ with $0<x<0.70$ is similar to that found for $Cd_xHg_{1-x}Te$.[34] In the latter case, however, the Γ's exhibit maxima for $x\simeq 0.8$. Unfortunately, because of the solubility limit, we cannot find out for $Cd_{1-x}Mn_xTe$ whether maxima also exist. In this case the total increase in Γ from $x=0$ to $x=0.70$ is $\simeq$300 meV, while for $Cd_xHg_{1-x}Te$ it is, in the same x range, less than 100 meV. Thus the possibility exists that the increase in the Γ's found for $Cd_{1-x}Mn_xTe$ is due to the repulsion of the $L_{4,5}$-L_6 valence by the $3d$ states (Fig. 10) which should be larger at L than inside the

Brillouin zone. This should *inhomogeneously* broaden the E_1 and $E_1+\Delta_1$ structures, the latter more than the former, in agreement with the results of Fig. 6. Such broadening would not be expected for E_0.

The phase angles ϕ (Fig. 7) were obtained from the fits of the second-derivative spectra of the E_1 and $E_1+\Delta_1$ critical points with Eq. (2). A phase angle ϕ has been used in the literature[26,33,34] as a phenomenological measure of excitonic effects in the line shapes. Such correlation can only be theoretically justified, on the basis of the Slater-Koster exciton potential, if ϕ turns out to be small.[31,39] This is not the case for the data of Fig. 7, especially for small x. Nevertheless, Eq. (2) seems to give a good representation of the critical points and the dependence of ϕ on x shown in Fig. 7 is reasonable if ϕ is a measure of the excitonic effects: they should become smaller with increasing disorder and thus reach a minimum for $x\simeq 0.5$. A similar behavior has been found for the $Cd_xHg_{1-x}Te$ system.[34] The parameters A of Eq. (2) represent the strength of the critical points. We have found them to be nearly independent of x. They are 2.85 ± 0.27 for E_1 and 2.30 ± 0.40 for $E_1+\Delta_1$.

V. CONCLUSIONS

We have measured with ellipsometry the (pseudo-) dielectric function of several $Cd_{1-x}Mn_xTe$ alloys in the visible, near infrared (ir), and near ultraviolet (uv). From a fit to the second-derivative spectra with Eq. (2) we have obtained the energies, strengths, Lorentzian broadenings, and excitonic phase angles of the E_1 and $E_1+\Delta_1$ critical points. Similar fits have also yielded information for the E_0 and E_2 critical points. The analysis of the dependence of the E_1, $E_1+\Delta_1$, and E_0 critical-point energies on x has given evidence for a hybridization of the top valence bands with the $3d$ states of Mn.

Note added in proof. Photoemission measurements with synchrotron radiation have recently shown that the unhybridized one-electron $3d\uparrow$ levels of Mn in $Cd_{1-x}Mn_xTe$ lie 3.5 eV below the top of the valence band [M. Taniguchi, L. Ley, R. L. Johnson, J. Ghijsen, and M. Cardona (unpublished)].

ACKNOWLEDGMENTS

We are grateful to R. R. Gałazka of the Institute of Physics, Warsaw, Poland, for the samples and also to W. Gebhardt (Regensburg, Federal Republic of Germany) for supplying one of the samples used in these measurements and for helpful discussions. We also thank L. Viczian for performing x-ray powder measurements to determine the composition of the alloys and W. Gebhardt for a critical reading of the manuscript.

*On leave from First Laboratory of Physics, Aristotle University of Thessaloniki, Thessaloniki, Greece.

†Present address: IBM Thomas J. Watson Research Center, P.O. Box 218, Yorktown Heights, NY 10598.

[1]A. Fazzio, M. J. Caldas, and A. Zunger, Phys. Rev. B **30**, 3430 (1984), and references therein.

[2]H. E. Gumlich, R. L. Pfrogner, J. C. Shaffer, and F. W. Williams, J. Chem. Phys. **44**, 3929 (1966); D. Langer and S. Ibuki, Phys. Rev. **138**, A809 (1965).

[3]K. C. Hass and H. Ehrenreich, J. Vac. Sci. Technol. **A1**, 1678 (1983).

[4]K. C. Hass, Ph.D. thesis, Harvard University, 1984.

[5]W. Zahorowski and E. Gilberg, Solid State Commun. **52**, 921 (1984).

[6]N. Bottka, J. Stankiewicz, and W. Giriat, J. Appl. Phys. **52**, 4189 (1981).

[7]R. T. Delves and B. Lewis, J. Phys. Chem. Solids **24**, 549 (1963).

[8]J. K. Furdyna, W. Giriat, D. F. Mitchell, and G. I. Sproule, J. Solid State Chem. **46**, 349 (1983).

[9]A. Goldman, Phys. Status Solidi B **81**, 9 (1977).

[10]M. Podgorny and J. Oleszkiewicz, J. Phys. C **16**, 2547 (1983).

[11]R. O. Bell, Rev. Phys. Appl. **12**, 391 (1977).

[12]N. T. Khoi and J. A. Gaj, Phys. Status Solidi B **83**, K133 (1977).

[13]J. Stankiewicz, N. Bottka, and W. Giriat, J. Phys. Soc. Jpn. Suppl. **49**, 827 (1980).

[14]M. El Amrani, J. P. Lascaray, and J. Diouri, Solid State Commun. **45**, 351 (1983); J. Diouri, J. P. Lascaray, and R. Triboulet, *ibid.* **42**, 231 (1982).

[15]P. Lemasson, B. L. Wu, R. Triboulet, and J. Gautron, Solid State Commun. **47**, 669 (1983).

[16]N. E. Christensen, Phys. Rev. B **30**, 5753 (1984).

[17]E. Müller, W. Gebhardt, and W. Rehwald, J. Phys. C **16**, L1141 (1983).

[18]W. Shan, S. C. Shen, and H. R. Zhu, Solid State Commun. (to be published).

[19]J. E. Morales-Toro, W. M. Becker, B. I. Wang, U. Debska, and J. W. Richardson, Solid State Commun. **52**, 41 (1984).

[20]T. Kendelewicz, Solid State Commun. **36**, 127 (1980).

[21]M. Zimnal-Starnawska, M. Podgorny, A. Kisiel, W. Giriat, M. Demianiuk, and J. Zmija, J. Phys. C **17**, 615 (1984).

[22]R. Bücker, H. E. Gumlich, and M. Krause, J. Phys. C **18**, 661 (1985).

[23]M. Cardona and D. L. Greenaway, Phys. Rev. **131**, 98 (1963).

[24]*Physics of II-VI and I-VII Compounds, Semimagnetic Semiconductors,* Vol. 17 of *Landolt-Börnstein: Numerical Data and Functional Relationships in Science and Technology,* edited by O. Madelung (Springer, Berlin, 1982), part b.

[25]D. E. Aspnes, Opt. Commun. **8**, 222 (1973); D. E. Aspnes and A. A. Studna, Appl. Opt. **14**, 220 (1975).

[26]L. Viña and M. Cardona, Phys. Rev. B **29**, 6739 (1984).

[27]D. E. Aspnes, J. Vac. Sci. Technol. **17**, 1057 (1980).

[28]N. M. Bashara and R. M. Azzam, in *Ellipsometry and Polarized Light* (North-Holland, Amsterdam, 1977).

[29]A. Savitzky and J. E. Gollay, Anal. Chem. **36**, 1627 (1974); J. Steinier, Y. Termonia, and J. Deltour, *ibid.* **44**, 1906 (1972).

[30]D. E. Aspnes, J. Opt. Soc. Am. **64**, 639 (1974); D. E. Aspnes and A. A. Studna, Phys. Rev. B **27**, 985 (1983).

[31]M. Cardona, *Modulation Spectroscopy,* in Supplement 11 of *Solid State Physics,* edited by F. Seitz, D. Turnbull, and H. Ehrenreich (Academic, New York, 1969).

[32]Y. Toyozawa, M. Inoue, T. Inui, M. Okazaki, and E. Hanamura, J. Phys. Soc. Jpn. **22**, 1337 (1967).

[33]J. E. Rowe and D. E. Aspnes, Phys. Rev. Lett. **25**, 162 (1970).

[34]L. Viña, C. Umbach, M. Cardona, and L. Vodopyanov, Phys.

Rev. B **29**, 6752 (1984).
[35]K. Saito, A. Ebina, and T. Takahashi, Solid State Commun. **11**, 841 (1972).
[36]J. R. Chelikowsky and M. L. Cohen, Phys. Rev. B **14**, 556 (1976).
[37]B. Velicky, Jan Masek, G. Paolucci, V. Chab, M. Surman, and K. C. Prince, in *Advances in Solid State Physics,* edited by P. Grosse (Pergamon-Vieweg, Oxford-Braunschweig, in press).
[38]M. Cardona, Phys. Rev. **129**, 69 (1963).
[39]Y. Toyozawa, M. Inoue, T. Inui, M. Okazaki, and E. Hanamura, J. Phys. Soc. Jpn. Suppl. **21**, 133 (1966).